Increasing of malignancy of breast cancer cells after cryopreservation: molecular detection and activation of angiogenesis after CAM-Xenotransplantation.

Xin Du
Uniklinik Koln
P. Todorov
Institut po Biologija i imunologija na razmnozavaneto Akademik Kiril Bratanov Balgarska akademija na naukite
Evgenia Isachenko
Uniklinik Koln
G Rahimi
Uniklinik Koln
P. Mallmann
Uniklinik Koln
Yuanguang Meng
PLA General Hospital
Vladimir Isachenko (vladimir.isachenko@gmail.com)
Cologne University https://orcid.org/0000-0002-3674-543X

Research article

Keywords: Cryopreservation; Breast cancer; Epithelial-mesenchymal transition; Cell motility; Angiogenesis; Chorioallantoic membrane

Posted Date: June 22nd, 2020

DOI: https://doi.org/10.21203/rs.3.rs-26913/v1

Version of Record: A version of this preprint was published on August 12th, 2020. See the published version at https://doi.org/10.1186/s12885-020-07227-z.

Abstract

Background: Ovarian tissue cryopreservation has a wide range of cancerous indications. Avoiding relapse becomes a specific area of concern that clinicians frequently encounter. The data about the comparative viability of cancer cells after cryopreservation are limited. This study aimed to evaluate the effect of cryopreservation on breast cancer cells.

Methods: Samples were prepared using ZR-75-1 and MDA-MB-231 cell lines and divided into cryopreserved and non-intervened groups, respectively. Biological properties and the related protein markers were investigated. Cell morphology was monitored under the microscope. Cell proliferation, migration, and invasion were characterized by CCK-8, wound-healing, and transmembrane assay, respectively. The expression of Ki-67, P53, GATA-3, E-cadherin, Vimentin, and F-Actin was measured by immunofluorescent staining and western blotting. Xenotransplantation was established on the chorioallantoic membrane (CAM) culture system to explore angiogenesis close to the grafts.

Results: Lamellipodia and filopodia were observed in cryopreserved ZR-75-1 cells. Both cell lines demonstrated increased cell motility and invasive ability after cryopreservation. However, cell proliferation was invariable in accordance with a regular expression of Ki-67 and P53. In ZR-75-1 cells, data exhibited a downregulation of E-cadherin after the decreased expression of GATA3, indicating the loss of intercellular adhesion after cryopreservation. Vimentin and F-actin were both upregulated in cryopreserved sample cells. Angiogenesis in CAM was significantly activated by cryopreserved MDA-MB-231 cells.

Conclusions: Cryopreservation causes an increasing malignancy of ZR-75-1 and MDA-MB-231 cells and thus raises the risk of metastasis.

Background

With the aim of fertility preservation, ovarian tissue cryopreservation (OTC) is at present the medical treatment of a stable increase of the using intensity [1]. The beneficiaries include girls and patients diagnosed with malignant diseases including but not limited to gastrointestinal carcinoma, leukemia and breast cancer [1, 2]. Clinicians fear for the existence of disseminated cancer cells that are dormant in the ovaries before anti-cancer treatment [3]. However, data about effect of cryopreservation procedure on viability of cancer cells are limited.

As reported, cryopreservation adversely affected the decidualization potential and cytokine production of human endometrial stromal cells [4]. The activity of xenobiotic metabolizing enzymes and responsiveness to enzyme-inducing agents reduced in cryopreserved human hepatocytes compared with that in freshly isolated cells[5]. However, cryopreserved umbilical cord blood mononuclear cells (UCB-MNCs) exhibit similar properties to those of fresh UCB in vitro and in vivo [6]. Endothelial progenitor cells derived from UCB-MNCs induced responses to cytokines and recovery of carotid artery injury analogous with those from peripheral blood of healthy volunteers [7].

Optimization of procedures of cryopreservation has an aim to improve the viability of post-thawing cells [8–10]. Concurrently, the vitality of veiled or dormant cancer cells should not be neglected. Concealed disseminated cancer cells are asymptomatic and are thought to be growth-arrested in G0 to G1 of cell cycle and thus in a quiescent state during the freezing process. These cells evade the immune response and are untreatable due to drug resistance[11].

This study aimed to evaluate the effect of cryopreservation on ZR-75-1 and MDA-MB-231 human breast cancer cells in the form of compacted fragments (as a model of solid tumors).

Methods

Cell lines and culture

Except where otherwise specified, all reagents were obtained from Sigma (Sigma Chemical Co., St. Louis, USA).

All manipulations described below were repeated 82 times: 82 cell culture dishes with monolayer were formed, and 82 compacted fragments were formed (47 from ZR-75-1 cells and 35 from MDA-MB-231 cells).

Cells of ZR-75-1 and MDA-MB-231 were purchased from American Type Culture Collection (ATCC; Manassas, USA) and grown in AIM V Medium (Thermo Fisher Scientific, Waltham, USA) supplemented with 10% fetal bovine serum (FBS) and Amphotericin B at 37 °C in a humidified chamber with 5% CO_2. Culture media were renewed every 48 h.

Formation of the model of solid tumors from monolayer was previously described [12]. Briefly, the cells after three times of cell passages were in vitro cultured for ten days without cell passages. Culture medium was renewed every 24 h after a cell layer was formed. A cell scraper (Greiner Bio-one, Frickenhausen, Germany) was used for harvesting the cell layer and forming the model tissue for the following cryopreservation. This method was applied as well to the cryopreserved cells back to in vitro culture, albeit without cell passage, before xenotransplantation of the chorioallantoic membrane.

Cryopreservation (freezing and thawing) of the model tissues

Cryopreservation of compacted fragments of cancer cells was performed based on the protocols for cryopreservation of fragments of human ovarian tissue [13] with adjustment and peculiarities as described below. The model tissues were cryopreserved similarly to the process for ovarian fragments.

The harvested tissues were placed for 5 min (ZR-75-1 cells) and 10 min (MDA-MB-231 cells) into the standard 5 ml cryo-vials (Thermo Fisher Scientific, Rochester, USA) previously filled by 4.5 ml freezing solutions (medium L-15 supplemented with 6% dimethyl sulfoxide, 6% ethylene glycol and 0.15 M sucrose) precooled to 4 °C. Then compacted cells tissues were frozen in IceCube 14S freezer (SyLab,

Neupurkersdorf, Austria). The slow cooling profile started at -6 °C, the samples were then cooled from − 6 to -34 °C at a rate of -0.3 °C/min. The used freezing protocol included auto-seeding step at -6 °C. At -34 °C cryo-vials were finally plunged into liquid nitrogen and stored until thawing.

For thawing of samples, cryo-vials were removed from liquid nitrogen and held for 30 s at room temperature, they were then immersed in a 100 °C (boiling) water bath for 60 s. The exposure time in the boiling water was visually controlled by the presence of ice in the medium; as soon as the ice was in form of 2 to 1 mm apex, the cryo-vial was removed from the boiling water, at which point the final temperature of the medium was between 4 and 10 °C. Within 10 s after thawing, about 90% of freezing medium was removed from cryo-vials and then these cryo-vials were filled by thawing solution pre-warmed to 37 °C (basal medium containing 0.5 M sucrose). Then cryo-vials were put into thermostat at 37 °C for 7 min (ZR-75-1 cells) and for 15 min (MDA-MB-231 cells) for stepping removal of cryoprotectants. After dehydration, about 90% of thawing medium (0.5 M sucrose) was removed from cryo-vial and then these cryo-vials were filled step wisely by basal (culture) medium. For stepwise rehydration (slow addition of basal medium to the solution of sucrose with cells), it was used the same, previously published 'dropping' methodology [14]. The final concentration of sucrose was 0.05 M, resulting in almost isotonic conditions. After rehydration, cells were digested by 6 ml 0.05% Trypsin-EDTA, 5 min at 37 °C in a humidified chamber with 5% CO_2. After washing and centrifuged, the cell pellet was resuspended in 10 ml culture medium by full pipette and then transferred into a 10 cm cell culture dish to allow adhesion overnight.

Observation of cell growing and morphology

Cryopreserved ZR-75-1 and MDA-MB-231 cells were seeded in AIM V medium and at a concentration of 1×10^4 cells/ml in 96-well plates compare with the controls, respectively. Cells were allowed to adhere overnight. We measured cell growing by using Cell Counting Kit-8 (CCK-8) and observed consecutively for five days. From day 1 to 5, ten µl CCK-8 solution was added to each well of one plate at a fixed time and incubated for 4 h, then the OD at 450 nm (reference 650 nm) was determined by a multimode reader machine (Tecan Group Ltd., Maennedorf, Zurich, Switzerland). Culture media were renewed every 48 h. Results were plotted with the time axis as the abscissa and the cell count as the vertical axis. Each experiment was repeated three times. For the morphology change, cells were maintained in the 10 cm culture dish to observe under microscopy each day. Images were taken by EVOS FL Auto 2 Cell Imaging System (Thermo Fisher Scientific).

Assessment of cell motility

Cell motility was determined using thewound-healing assay and 3D transmembrane migration and invasion experiment. The wound-healing test was implemented with a well-established artificial gap on the confluent cell monolayer. A density of 1×10^6 cells/ml in 140 µl suspension of both cell lines was seeded in a 35 mm µ-Dish ibidi Culture Insert (ibidi GmbH, Planegg, Bavaria, Germany) with 70 µl in each well, incubated for 24 h and obtained the cell layers. After removal of the insert, the µ-Dish was washed with PBS twice to remove cell debris and non-attached cells and filled with 2 ml of 1% FBS-supplemented cell-free medium. Time-lapse measurement of the wound area between the cell layers was performed

every 24 h for ZR-75-1 and every 2 h for MDA-MB-231 cells to calculate cell front velocity. Experiments were carried out in triplicate at least three times.

Cell invasion was determined in vitro to evaluate the ability of tumor cells to transmigrate a layer of the reconstructed extracellular matrix. Corning transwell inserts were used to accomplish the cell invasion assay, according to our previous study [12]. Polycarbonate filters (6.5 mm in diameter, 8 μm pore size) were coated with type I rat tail collagen (100 μg/ml; BD Biosciences, Franklin Lakes, USA) for 1 h at 37 °C by the manufacturer's protocol. The fresh and cryopreserved cells were resuspended and seeded into the upper compartment of the insert in the serum-free culture medium, respectively. ZR-75-1 cells were seeded at 2×10^5 cells/well and cultured for 72 h; MDA-MB-231 cells were seeded 5×10^4 cells/well and cultured for 8 h. The lower chamber was filled with 600 μl of the appropriate culture medium supplemented with FBS as a chemoattractant. After incubation, the upper insert with cells was washed with PBS, fixed with 4% formaldehyde, and permeabilized with methanol at room temperature. Cells were then stained with 0.1% crystal violet solution and were gently rinsed with PBS and wiped by cotton-tipped swabs then dried in the air. Penetrative cells went through the polymerized collagen layer to the bottom of the polycarbonate membranes and were counted in five different fields of view under a microscope. For the migration assay, cells were treated using the same procedure, except that the transwell membrane was not coated with collagen. Samples in each group ran in triplicate. Each experiment was performed at least three times.

Immunofluorescent (IF) staining

Antibodies were purchased from Biolegend. Twenty-five $\times 10^4$ cells were first seeded on cover glasses in 6-well plates. After 48 h, the culture medium was aspirated, and cells were fixed with 2% paraformaldehyde for 20 min at room temperature. After washing twice by PBS, the cells were incubated in 0.5% Triton X-100 in PBS for 10 min for permeabilization and blocked by cell staining buffer (Biolegend, San Diego, USA) for 30 min. Then the coverslips were transferred into a humidified chamber and incubated with Alexa Fluor 488-conjugated anti-human Ki-67 antibody, Alexa Fluor 594 anti-human Epithelial cadherin (E-cadherin) antibody, Alexa Fluor 647 anti-GATA3 antibody and Alexa Fluor 488 anti-Vimentin antibody overnight at 4 °C, or with Alexa Fluor 488-conjugated Flash Phalloidin (F-Actin) in room temperature for 1 h. After washing twice, the coverslips were mounted on glass slides with 25 μl of mounting medium with 4',6-diamidino-2-phenylindole (Abcam, Cambridge, UK). The slides were analyzed by a Leica SP8 confocal microscope. Images were taken using LAS X software (Leica Microsystems, Wetzlar, Germany).

Western blotting (WB)

Cultured cells were incubated in Accutase at 37 °C for 5–10 min followed by resuspension and centrifugation. Cell lysis was conducted using lysis buffer: RIPA buffer (Thermo Fisher Scientific) with protease inhibitor cocktail. Cell lysates were separated by centrifuging at 20000 g, 30 min at 4 °C. Protein concentrations were measured via Bradford test and adjusted to 20 μg/20 μl in one sample by 4X sodium dodecyl sulfate-containing laemmli sample buffer, then heated in boiling water for 5 min. Later, sodium

dodecyl sulfate-polyacrylamide gel electrophoresis (SDS-PAGE) was applied to separate the total protein and then separated protein was transferred on nitrocellulose membrane. We used the pre-cast 4–12% polyacrylamide gradient gels (Thermo Fisher Scientific) and the Trans-Blot® Turbo™ Turbo membrane (Biorad, Hercules, USA) in the transfer system according to the manufacturer instruction. After blocking, the membrane was incubated in primary antibodies diluted to 1:2000 by 5% Bovine Serum Albumin in PBST (0.1% Tween-20 in PBS), at 4 °C overnight. The P53, E-cadherin, GATA3, and Vimentin antibodies were purchased from Cell Signaling Technologies (Danvers, Massachusetts, USA). The following day, the fluorescent secondary antibodies (LI-COR, Lincoln, NE, USA) were used to incubate at room temperature for 2 h. Bands were visualized using Odyssey Clx (LI-COR). Image J software (http://developer.imagej.net) was used to estimate the band density.

Model of solid tumors tissue CAM-Xenotransplantation: stimulation of angiogenesis

Preparation of the chick embryo chorioallantoic membrane (CAM) for transplantation of cancer cells were performed as described early [15, 16]. Briefly, fertilized eggs of White Leghorn chickens were purchased at a local hatchery and incubated at 37 °C-38 °C with 60% relative humidity for three days. On day 5, each egg was washed with warm 70% ethanol and opened a small window with 1.0 cm diameter on the sharp pole of the shell. We sealed the window by a 2 × 2 cm medical fabric tape only on the edge of the opening, and the egg was allowed to continue the incubation. The following day, a 1-mm-thick sterile silicone ring with an inner diameter of 5 mm was laid on the exposed chorioallantoic membrane. We divided 54 well-incubated 6-day-old chicken embryos randomly into four groups, 12 eggs in each group, and six as blank controls. Both initial and cryopreserved MDA-MB-231 model tissues were adjusted to two concentrations: 4×10^6 and 8×10^6 cells/egg. Then we grafted the four groups of tissues into pre-treated chicken embryos on the relative avascular region of CAM, which was group 1: 4×10^6 fresh cells; group 2: 8×10^6 fresh cells; group 3: 4×10^6 cryopreserved cells; group 4: 8×10^6 cryopreserved cells. We used 40 μl PBS as blank. The five-millimeter inner diameter silicon rings were used to restrict the displacement of the grafts along with the chick embryo movement. The medical tape closed the window and continued to incubate for six days. The survival of the embryos, the tumor formation rate and the induction of angiogenesis were observed. The tumors with a diameter of ≥ 0.3 cm was considered positive, and the tumor formation rate was calculated. At the same time, the CAM xenograft specimens were fixed in situ with 4% paraformaldehyde and removed. The neovascularization in the tumor area was observed under a microscope on the 6th day of in vivo culture. The field of blood vessels distributed radially within a radius of 1 cm from the tumor tissue was quantified by Image J software. The relative density of blood vessels was calculated by the formula: Vascular density = vascular area/CAM area. Tumor volume was measured under an inverted microscope by the formula: Tumor volume = 1/2 × (major axis × minor axis^2).

Statistical analysis

Data analysis was executed with SPSS 23.0 software (IBM Corp., Armonk, USA). Differences among the groups were tested by Student's t-test or two-way ANOVA. Data are expressed as mean ± standard deviation. The level of statistical significance was set at $p < 0.05$.

Results

Cell growing is invariable after cryopreservation

After 5-day in vitro culture, cryopreserved ZR-75-1 cells reached a concentration of 15.7×10^4 cells/ml, and that of cryopreserved MDA-MB-231 cells was 25.1×10^4 cells/ml. It was noted no significant differences compared with the two lines before cryopreservation (ZR-75-1: 14.4×10^4 cells/ml, MDA-MB-231: 26.6×10^4 cells/ml), respectively, $p > 0.05$.

ZR-75-1 cells exhibit morphology change

We observed that a number of ZR-75-1 cells displayed morphology change from the typical grape-like cluster to fibroblast-like or spindle-shaped, and dissociated from the nearby cell mass. The generated filopodia and lamellipodia were demonstrated in Fig. 1. The compelling morphology changes are associated with enhanced cell motility. Such differences were difficult to recognize under the microscope in the cultured cryopreserved MDA-MB-231 cells, due to its original morphology.

Cryopreservation increases migrating and invasive ability of the cancer cells

The gap closure of the cryopreserved cells was significantly more rapid than that of the control cells, $p < 0.05$. Cryopreserved cancer cells of both lines exhibited more intensive transmembrane migrating and invasive ability in comparison with fresh cells, $p < 0.001$, shown in Fig. 2.

Cryopreservation regulates the expression of protein Ki-67 and P53

Accordingly, the expression of multiple related proteins was investigated as evidence of the phenotypes of cryopreserved breast cancer cells. The IF staining and WB of Ki-67 and P53, respectively, in ZR-75-1 and MDA-MB-231 cells. By calculating the Ki-67-positive cells, it was found that the proportion of positive cells decreased after cryopreservation, showing 50.7% vs. 45.0% in ZR-75-1 cells, and 82.6% vs. 79.6% in MDA-MB-231 cells. The expression of P53exhibited no statisticaldifference in cells before andafter cryopreservation, $p > 0.05$.

Cryopreservation inducesloss of intercellular adhesion

Fresh ZR-75-1 cells expressed GATA3 more intensively than cryopreserved cells (Fig. 3). E-cadherin expression was associated with GATA3 level in ZR-75-1 cells. The signals significantly attenuated after

cryopreservation, $p < 0.001$ (Fig. 4). The expression of E-cadherin was downregulated after cryopreservation in MDA-MB-231 cells. However, since this cell line was of triple-negative molecular subtype, thus the signals by IF and WB were weak, and GATA3 expression was low or utterly lost.

Cryopreservation strengthens cell motility by upregulating Vimentin and F-Actin

In fresh ZR-75-1 cells, the expression of Vimentin was at a low level. It increased significantly after cryopreservation (from $p < 0.01$ to $p < 0.0001$). In fresh MDA-MB-231 cells, Vimentin was well detectable and the level continued to be upregulated after cryopreservation, $p < 0.0001$. F-Actin was visualized by IF analysis. The expression level of F-Actin in ZR-75-1 and MDA-MB-231 cells increased significantly after cryopreservation, $p < 0.0001$ (Fig. 5).

Cryopreservation stimulates angiogenesis and tumor growth

The survival rate of eggs inoculated by the initial cells was > 90%, and that of the two groups inoculated by cryopreserved cells was > 80%, $p > 0.05$. The tumor formation rate was > 90% for both fresh and cryopreserved cancer cells, $p > 0.05$.

There was no difference in blood vessel morphology, which was smooth and equably distributed between the inoculated and non-inoculated areas of the blank. In group 1, 2, 3 and 4, xenograft sites showed the radial distribution of blood vessels and an escalation of the surrounding vasculature. In comparison with the fresh-cell groups, the groups of cryopreserved cells showed distinct growth of capillaries into the tumor tissue, an increasednumber of peripheral blood vessels, and exhibited a coarse dendritic configuration (Fig. 6). The ratio between the vascular area and the CAM area of group 1, 2, 3 and 4 was 0.238 ± 0.05, 0.244 ± 0.03, 0.313 ± 0.03 and 0.342 ± 0.04, respectively. Thus, the vascular density of groups with cryopreserved cells was higher than that of the groups with fresh cells, $p < 0.0001$. The variances of group 1 vs. group 2, and group 3 vs. group 4 were not statistically significant.

The tumor volume in groups 1, 2, 3 and 4 was 19.48 ± 3.07 mm^3, 22.61 ± 6.99 mm^3, 26.63 ± 6.44 mm^3, and 46.48 ± 9.35 mm^3, respectively. Tumor masses in group 1 and 2 were of small sizes, showing significant differences from those in group 3 and 4, $p < 0.05$. The tumor volume was higher in Group 4 compared with that in other three groups, respectively, $p < 0.0001$, revealing that tumor growth was associated with surrounded microenvironment and the autologous tumor burden.

Discussion

Ovarian tissue cryopreservation and the following transplantation have served as a fertility preservation approach for over a decade. More and more cancer survivors access this treatment for fertility restoration [17, 18]. The effect of cryopreservation on cell viability and genetic regulation has been thoroughly investigated on a variety of cell types [19], while the impact on cancer cells is largely unknown. Our study

is the first to characterize the phenotypes and molecular changes of breast cancer cell lines undergoing the process of cryopreservation.

Here, we tested ZR-75-1 cells of luminal A and aggressive MDA-MB-231 cells of triple negative molecular subtype. To prevent intracellular crystallization during the process of cryopreservation, we used permeable cryoprotectants to protect the cells. The main cryoprotectants are high molecular alcohols: glycerol, ethylene glycol and, propylene glycol, as well as dimethyl sulfoxide (DMSO). The 'protective' component is usually 10 to 12% of the total solution and is either a single ingredient (DMSO) or a mixture of DMSO and the other one of the glycols [20]. In our protocol, we used mixture of two cryoprotectants which we used to protect ovarian fragments included at least five types of cells. By our data, protective effect of 12% DMSO was lower than that of 12% multi-cryoprotectant solution (V. Isachenko, not published data). In this study, we further proved that cryopreservation using multi-cryoprotectants did not suppress cell growing ability reflected in the expression of Ki-67 and P53 in the cryopreserved and fresh breast cancer cells.

Epithelial-to-mesenchymal transition (EMT)is a reversible process, during which epithelial cells lose intercellular adherence and gain migratory and invasive properties to transdifferentiate to mesenchymal cells. We observed the decreased expression of GATA3 and E-cadherin in the cryopreserved cells. GATA3 functions as a critical transcriptional activator of E-cadherin to impede the phenotype transition between epithelial and mesenchymal cells, and suppresses metastasis and alters the tumor microenvironment in breast cancer [21]. E-cadherin is responsible for cell-cell adhesion. Wild-type E-cadherin downregulation is related to the reduction of intercellular adhesion [22]. Loss of E-cadherin is considered to be an elemental event in the process of EMT, which played a vital role in cancer metastasis [23]. It was reported that the expression of E-cadherin was suppressed in GATA3-knockout MDA-MB-231 cells [24]. Our data illustrated that the expression level of E-cadherin in ZR-75-1 cells was correlated to that of GATA3.

Vimentin and actin form the intermediate filament and microfilament, respectively, and participate in cell motility. Vimentin is the major cytoskeletal component of mesenchymal cells. F-actin also engages in the maintenance of cell shape. Since the induction of cell motility is considered to be the second phase of EMT [25, 26], we evaluated these two cytoskeleton proteins to reveal the mechanism of the enhanced cell moving after cryopreservation. Our data indicated that cryopreservation induced the improved migratory and invasive ability in breast cancer cells through upregulating the expression of Vimentin and F-actin and reorganization of intermediate filaments and microfilaments.

Angiogenesis is a vital process for tumor growth and spread. Our results revealed that cryopreserved breast cancer cells stimulated the generation of neovasculature. Subsequently, the cryopreserved grafts were of large volume after acquiring the newly established blood supply.

There are adverse effects observed at somatic cells cryopreservation: hypoxia is one of the most substantial effects together with intracellular Ca^{2+} concentration, osmotic disruption of cellular membranes, generation of reactive oxygen species, and lipid peroxidation [27]. Cryopreserved cancer cells

experience an imbalance between oxygen delivery and consumption through the procedures of freezing and thawing. The condition of low oxygen tension activates the hypoxia-inducible factors (HIFs), increases the permeability of mitochondrial membrane, causes mitochondrial swelling [28, 29], and enhances malignant phenotypes of cancer cells, that are positively correlated to cancer metastasis [30]. The transcription factors HIFs mediate the primary responses to hypoxia [31, 32]. Thereby, we inferred that cryopreservation altered GATA 3 and E-cadherin expression through the activation of HIFs. HIFs also induce proteinases involved in the degradation of extracellular matrix to accelerate the invasion then affect cell motility corresponding to cell migration and invasion, which is the first step of metastasis cascade [31].

Cell migration is associated with the metabolism of cellular energy. By cryopreservation, HIFs activation and mitochondria swelling increase glycolysis and thus sustain cancer metastasis[33–35]. Calcium regulates focal adhesion turnover, cytoskeletal reorganization, and other processes of tumor cell movement through contacting with multiple downstream proteins [36]. Whether HIFs and mitochondria induce upregulation of Vimentin and F-actin still needs further research.

Tumors induce neovascularization by secreting various growth factors and proteinases [37, 38], several of which are the downstream proteins induced by HIFs. In addition, cancer cells cease mitosis and survive in dormancy under the condition of low temperature. A stable microvasculature constitutes dormant niches ofcancer cells[39]. Angiogenesis accelerates the growth of quiescent breast cancer cells [40].

Conclusions

Cryopreservation of ZR-75-1 and MDA-MB-231 human breast cancer cells lead to an increasing malignancy and thus raises the risk of metastasis.

Abbreviations

OTC: ovarian tissue cryopreservation;UCB-MNCs: umbilical cord blood mononuclear cells; FBS: fetal bovine serum; CCK-8: cell counting kit-8; IF: immunofluorescent; E-cadherin: epithelial cadherin; WB: western blotting;CAM: chorioallantoic membrane; SDS-PAGE: sodium dodecyl sulfate-polyacrylamide gel electrophoresis; DMSO: dimethyl sulfoxide; EMT: epithelial-to-mesenchymal transition; HIFs: hypoxia-inducible factors.

Declarations

Ethics approval and consent to participate

Not applicable.

Consent for publication

Not applicable.

Availability of data and material

The datasets used and/or analyzed during the current study are available from the corresponding author on reasonable request.

Competing interests

The authors declare that they have nocompeting of interest.

Funding

Not applicable.

Authors' contributions

XD, EI, and VI contributed to the conceptualization, methodology, and investigation.XD and PT performed data analysis and wrote the manuscript.GR, PM, and YM wrote review andediting. VI contributed to supervision and project administration. All authors read and approved the final manuscript.

Acknowledgements

Not applicable.

References

1. Macklon KT. Prevalence of deaths in a cohort of girls and women with cryopreserved ovarian tissue. Acta Obstet Gynecol Scand 2019.
2. Poirot C, Brugieres L, Yakouben K, Prades-Borio M, Marzouk F, de Lambert G, Pacquement H, Bernaudin F, Neven B, Paye-Jaouen A *et al*. Ovarian tissue cryopreservation for fertility preservation in 418 girls and adolescents up to 15 years of age facing highly gonadotoxic treatment. Twenty years of experience at a single center. Acta Obstet Gynecol Scand 2019.
3. Paez D, Labonte MJ, Bohanes P, Zhang W, Benhanim L, Ning Y, Wakatsuki T, Loupakis F, Lenz HJ. Cancer dormancy: a model of early dissemination and late cancer recurrence. Clinical cancer research : an official journal of the American Association for Cancer Research 2012; 18(3):645-53.
4. Bochev I, Belemezova K, Shterev A, Kyurkchiev S. Effect of cryopreservation on the properties of human endometrial stromal cells used in embryo co-culture systems. Journal of assisted reproduction and genetics 2016; 33(4):473-80.
5. Hengstler JG, Utesch D, Steinberg P, Platt K, Diener B, Ringel M, Swales N, Fischer T, Biefang K, Gerl M. Cryopreserved primary hepatocytes as a constantly available in vitro model for the evaluation of human and animal drug metabolism and enzyme induction. Drug Metab Rev 2000; 32(1):81-118.

6. Lin RZ, Dreyzin A, Aamodt K, Dudley AC, Melero-Martin JM. Functional endothelial progenitor cells from cryopreserved umbilical cord blood. Cell Transplant 2011; 20(4):515-22.
7. Yin Y, Liu H, Wang F, Li L, Deng M, Huang L, Zhao X. Transplantation of cryopreserved human umbilical cord blood-derived endothelial progenitor cells induces recovery of carotid artery injury in nude rats. Stem cell research & therapy 2015; 6:37.
8. Berkovitz A, Miller N, Silberman M, Belenky M, Itsykson P. A novel solution for freezing small numbers of spermatozoa using a sperm vitrification device. Human reproduction (Oxford, England) 2018; 33(11):1975-83.
9. Gallardo M, Paulini F, Corral A, Balcerzyk M, Lucci CM, Ambroise J, Merola M, Fernandez-Maza L, Risco R, Dolmans MM *et al*. Evaluation of a new freezing protocol containing 20% dimethyl sulphoxide concentration to cryopreserve human ovarian tissue. Reproductive biomedicine online 2018; 37(6):653-65.
10. Le MT, Nguyen TTT, Nguyen TT, Nguyen VT, Nguyen TTA, Nguyen VQH, Cao NT. Cryopreservation of human spermatozoa by vitrification versus conventional rapid freezing: Effects on motility, viability, morphology and cellular defects. European journal of obstetrics, gynecology, and reproductive biology 2019; 234:14-20.
11. Aguirre-Ghiso JA. Models, mechanisms and clinical evidence for cancer dormancy. Nat Rev Cancer 2007; 7(11):834-46.
12. Du X, Klaschik K, Mallmann P, Isachenko E, Rahimi G, Zhao Y, Bruns C, Isachenko V. An Experimental Model of Breast Cancer Cells: Informative Protocol for In Vitro Culture. Anticancer research 2018; 38(11):6237-45.
13. Isachenko V, Todorov P, Isachenko E, Rahimi G, Hanstein B, Salama M, Mallmann P, Tchorbanov A, Hardiman P, Getreu N *et al*. Cryopreservation and xenografting of human ovarian fragments: medulla decreases the phosphatidylserine translocation rate. Reproductive biology and endocrinology : RB&E 2016; 14(1):79.
14. Isachenko V, Montag M, Isachenko E, van der Ven K, Dorn C, Roesing B, Braun F, Sadek F, van der Ven H. Effective method for in-vitro culture of cryopreserved human ovarian tissue. Reprod Biomed Online 2006; 13(2):228-34.
15. Isachenko V, Mallmann P, Petrunkina AM, Rahimi G, Nawroth F, Hancke K, Felberbaum R, Genze F, Damjanoski I, Isachenko E. Comparison of In Vitro- and Chorioallantoic Membrane (CAM)-Culture Systems for Cryopreserved Medulla-Contained Human Ovarian Tissue. PLoS One 2012; 7(3):9.
16. Zeng YC, Tang HR, Zeng LP, Chen Y, Wang GP, Wu RF. Assessment of the effect of different vitrification solutions on human ovarian tissue after short-term xenotransplantation onto the chick embryo chorioallantoic membrane. Molecular reproduction and development 2016; 83(4):359-69.
17. Fabbri R, Macciocca M, Vicenti R, Paradisi R, Rossi S, Sabattini E, Gazzola A, Seracchioli R. First Italian birth after cryopreserved ovarian tissue transplantation in a patient affected by non-Hodgkin's lymphoma. International journal of hematologic oncology 2018; 7(4):Ijh08.

18. Ruan X, Du J, Korell M, Kong W, Lu D, Jin F, Li Y, Dai Y, Yin C, Yan S *et al*. Case report of the first successful cryopreserved ovarian tissue retransplantation in China. Climacteric 2018; 21(6):613-6.
19. Pogozhykh D, Pogozhykh O, Prokopyuk V, Kuleshova L, Goltsev A, Blasczyk R, Mueller T. Influence of temperature fluctuations during cryopreservation on vital parameters, differentiation potential, and transgene expression of placental multipotent stromal cells. Stem cell research & therapy 2017; 8(1):66.
20. Gook DA, Edgar DH: Ovarian tissue cryopreservation. In: *Principles and practice of fertility preservation*. Volume *2*, edn. Edited by Donnez J, Kim SS. New York: Cambridge University Press; 2011: 342-56.
21. Chou J, Lin JH, Brenot A, Kim JW, Provot S, Werb Z. GATA3 suppresses metastasis and modulates the tumour microenvironment by regulating microRNA-29b expression. Nat Cell Biol 2013; 15(2):201-13.
22. Rosso M, Lapyckyj L, Besso MJ, Monge M, Reventos J, Canals F, Quevedo Cuenca JO, Matos ML, Vazquez-Levin MH. Characterization of the molecular changes associated with the overexpression of a novel epithelial cadherin splice variant mRNA in a breast cancer model using proteomics and bioinformatics approaches: identification of changes in cell metabolism and an increased expression of lactate dehydrogenase B. Cancer & metabolism 2019; 7:5.
23. Yang J, Weinberg RA. Epithelial-mesenchymal transition: at the crossroads of development and tumor metastasis. Dev Cell 2008; 14(6):818-29.
24. Kim KS, Kim J, Oh N, Kim MY, Park KS. ELK3-GATA3 axis modulates MDA-MB-231 metastasis by regulating cell-cell adhesion-related genes. Biochem Biophys Res Commun 2018; 498(3):509-15.
25. Chen Y, Chen ZY, Chen L, Zhang JY, Fu LY, Tao L, Zhang Y, Hu XX, Shen XC. Shikonin inhibits triple-negative breast cancer-cell metastasis by reversing the epithelial-to-mesenchymal transition via glycogen synthase kinase 3beta-regulated suppression of beta-catenin signaling. Biochem Pharmacol 2019; 166:33-45.
26. Avtanski D, Garcia A, Caraballo B, Thangeswaran P, Marin S, Bianco J, Lavi A, Poretsky L. Resistin induces breast cancer cells epithelial to mesenchymal transition (EMT) and stemness through both adenylyl cyclase-associated protein 1 (CAP1)-dependent and CAP1-independent mechanisms. Cytokine 2019; 120:155-64.
27. Isachenko V, Todorov P, Isachenko E, Rahimi G, Tchorbanov A, Mihaylova N, Manoylov I, Mallmann P, Merzenich M. Long-Time Cooling before Cryopreservation Decreased Translocation of Phosphatidylserine (Ptd-L-Ser) in Human Ovarian Tissue. PLoS One 2015; 10(6):e0129108.
28. Hussain S. Measurement of Nanoparticle-Induced Mitochondrial Membrane Potential Alterations. Methods in molecular biology (Clifton, NJ) 2019; 1894:123-31.
29. Makarov VI, Khmelinskii I, Javadov S. Computational Modeling of In Vitro Swelling of Mitochondria: A Biophysical Approach. Molecules 2018; 23(4).
30. Hiraga T. Hypoxic Microenvironment and Metastatic Bone Disease. Int J Mol Sci 2018; 19(11).

31. Schito L, Semenza GL. Hypoxia-Inducible Factors: Master Regulators of Cancer Progression. Trends in cancer 2016; 2(12):758-70.
32. Rankin EB, Nam JM, Giaccia AJ. Hypoxia: Signaling the Metastatic Cascade. Trends in cancer 2016; 2(6):295-304.
33. Abd El-Hafez YG, Moustafa HM, Khalil HF, Liao CT, Yen TC. Total lesion glycolysis: a possible new prognostic parameter in oral cavity squamous cell carcinoma. Oral Oncol 2013; 49(3):261-8.
34. Zhao T, Zhu Y, Morinibu A, Kobayashi M, Shinomiya K, Itasaka S, Yoshimura M, Guo G, Hiraoka M, Harada H. HIF-1-mediated metabolic reprogramming reduces ROS levels and facilitates the metastatic colonization of cancers in lungs. Scientific reports 2014; 4:3793.
35. Zhang Y, Fang N, You J, Zhou Q. Advances in the relationship between tumor cell metabolism and tumor metastasis. Zhongguo Fei Ai Za Zhi 2014; 17(11):812-8.
36. Di J, Huang H, Qu D, Tang J, Cao W, Lu Z, Cheng Q, Yang J, Bai J, Zhang Y *et al*. Rap2B promotes proliferation, migration, and invasion of human breast cancer through calcium-related ERK1/2 signaling pathway. Scientific reports 2015; 5:12363.
37. Zhou R, Wang S, Wen H, Wang M, Wu M. The bispecific antibody HB-32, blockade of both VEGF and DLL4 shows potent anti-angiogenic activity in vitro and anti-tumor activity in breast cancer xenograft models. Exp Cell Res 2019; 380(2):141-8.
38. Thammineni KL, Thakur GK, Kaur N, Banerjee BD. Significance of MMP-9 and VEGF-C expression in North Indian women with breast cancer diagnosis. Mol Cell Biochem 2019.
39. Endo H, Inoue M. Dormancy in cancer. Cancer science 2019; 110(2):474-80.
40. Ghajar CM, Peinado H, Mori H, Matei IR, Evason KJ, Brazier H, Almeida D, Koller A, Hajjar KA, Stainier DY *et al*. The perivascular niche regulates breast tumour dormancy. Nat Cell Biol 2013; 15(7):807-17.

Additional File Legends

Supplementary Fig. 1

The uncropped western blots image of ZR-75-1 cells (round 1). It examined four proteins, including P53, E-cadherin, GATA3, and Vimentin, with 53kd, 125kd, 48kd, and 53kd of the expected molecular weight, respectively. The protein marker for P53 failed to develop specific signals. The whiteframes highlighted the cropped blots, labeled as in the manuscript.

Supplementary Fig. 2

The uncropped western blots image of ZR-75-1 cells (round 2). The relevant interpretation is the same as that of Supplementary Fig. 1. No blots were cropped.

Supplementary Fig. 3

The uncropped western blots image of ZR-75-1 cells (round 3). The relevant interpretation is the same as that of Supplementary Fig. 1. No blots were cropped.

Supplementary Fig. 4

The uncropped western blots image of MDA-MB-231 cells (round 1). It examined four proteins, including P53, E-cadherin, GATA3, and Vimentin, with 53kd, 125kd, 48kd, and 53kd of the expected molecular weight, respectively. The white frames highlighted the cropped blots, labelled as in the manuscript.

Supplementary Fig. 5

The uncropped western blots image of MDA-MB-231 cells (round 2). The relevant interpretation is the same as that of Supplementary Fig. 4.The white frames highlighted the cropped blots, labelled as in the manuscript.

Supplementary Fig. 6

The uncropped western blots image of MDA-MB-231 cells (round 3). The relevant interpretation is the same as that of Supplementary Fig. 4.No blots were cropped.

Supplementary Fig. 7

The cropped images of ZR-75-1 and MDA-MB-231 cells. **a**The cropped images of ZR-75-1 cells. The blots of E-cadherin, GATA3, Vimentin, and the relevant refences were cropped from supplementary fig. 1. **b**The cropped images of MDA-MB-231 cells.The blots ofGATA3, Vimentin, and the relevant refence protein Hsc70 were cropped from supplementary fig. 4.The blots of E-cadherin, and the relevant refence protein Hsc70 were cropped from supplementary fig. 5.

Figures

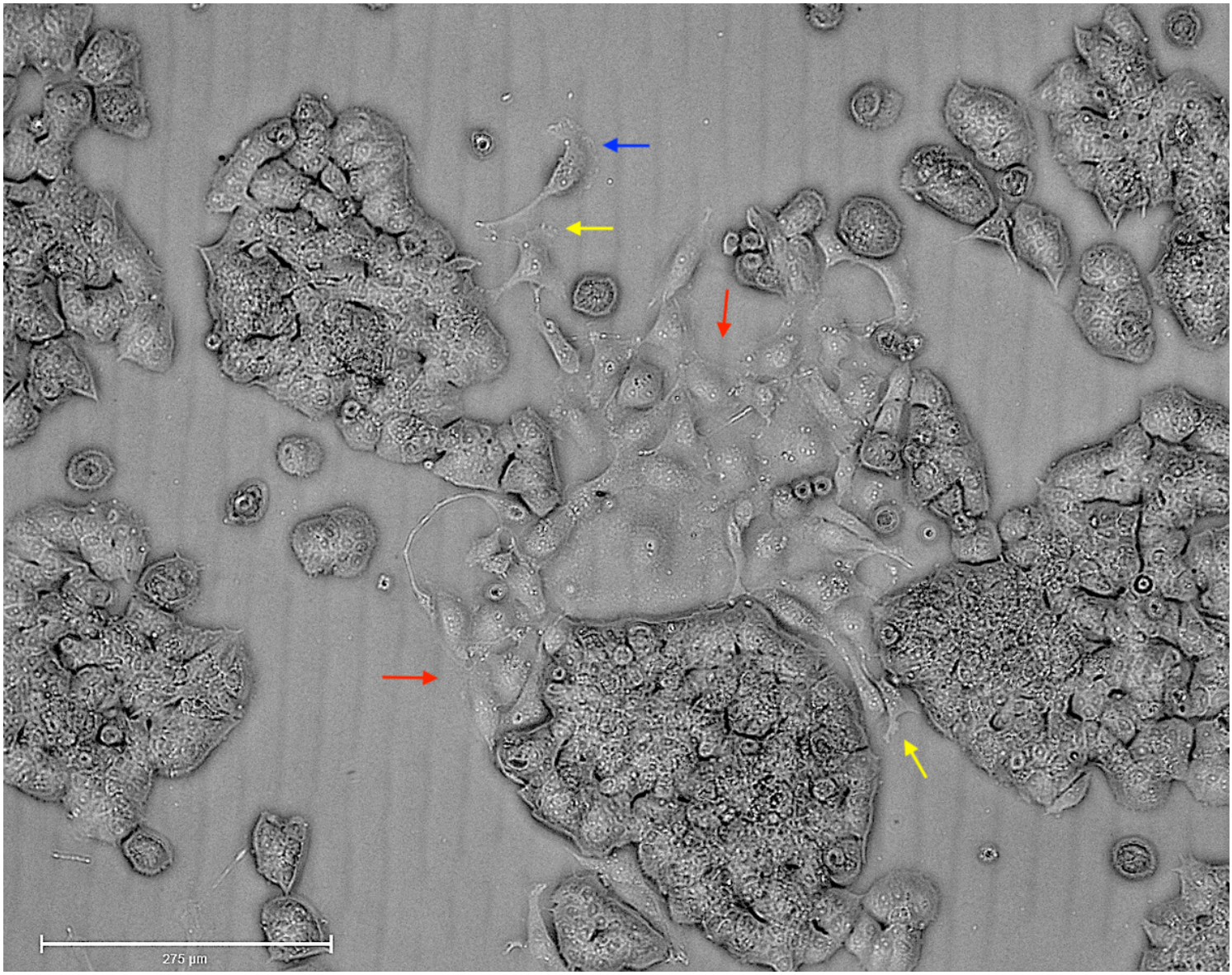

Figure 1

Morphological change of cryopreserved ZR-75-1 cells.The majority of ZR-75-1 cells stayed typical grape-like cluster. The red arrows pointed out the cells that were spindle-shaped and dissociated from the nearby cell masses. The blue and yellow arrows pointed out the lamellipodia and filopodia, respectively. Magnification ×150.

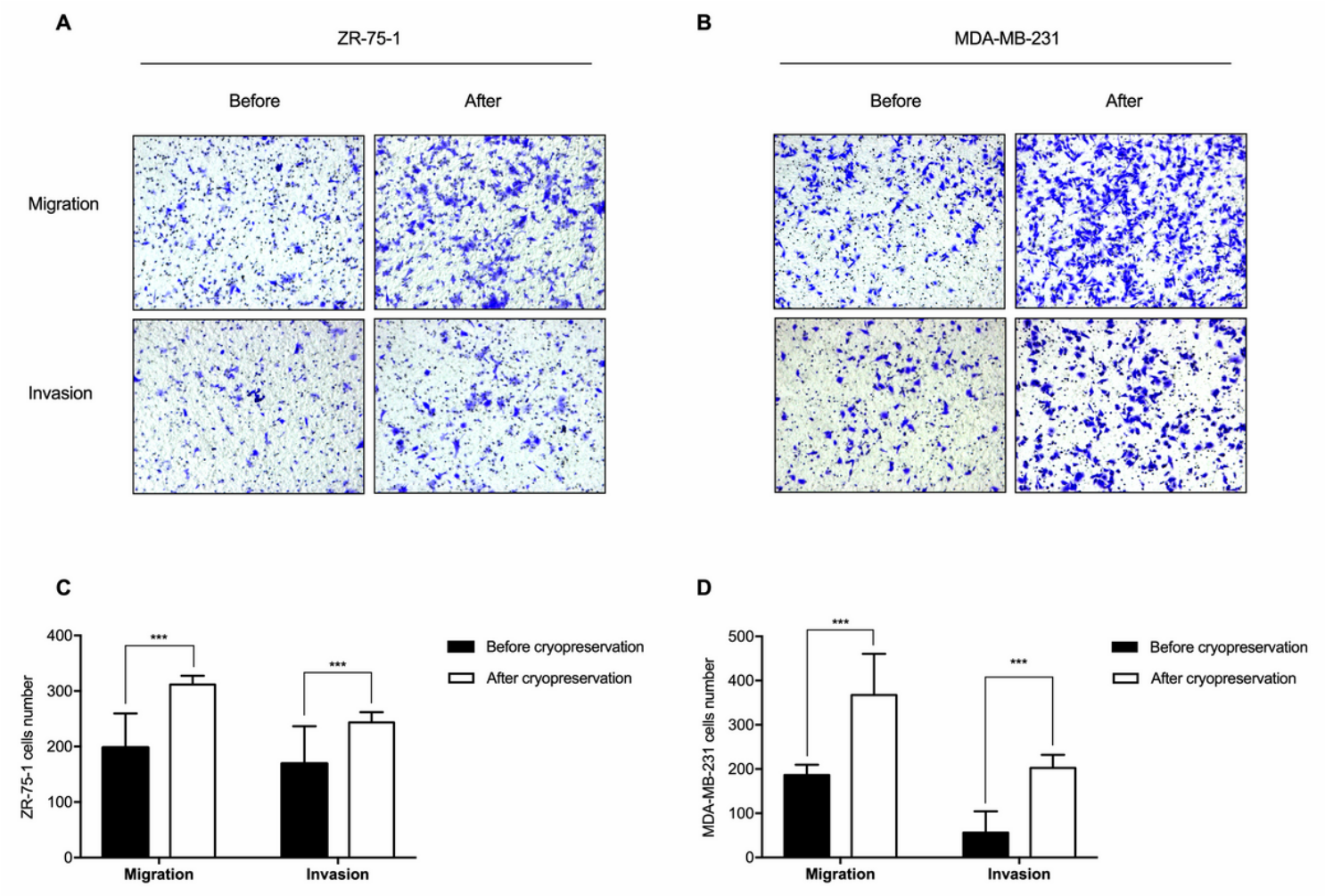

Figure 2

Increased transmembrane migration and invasion of cryopreserved breast cancer cells. a, c Transmembrane migration and invasion of ZR-75-1 cells before and after cryopreservation; b, d Transmembrane migration and invasion of MDA-MB-231 cells before and after cryopreservation. Magnification ×13.5. Significantly different at ***p<0.001.

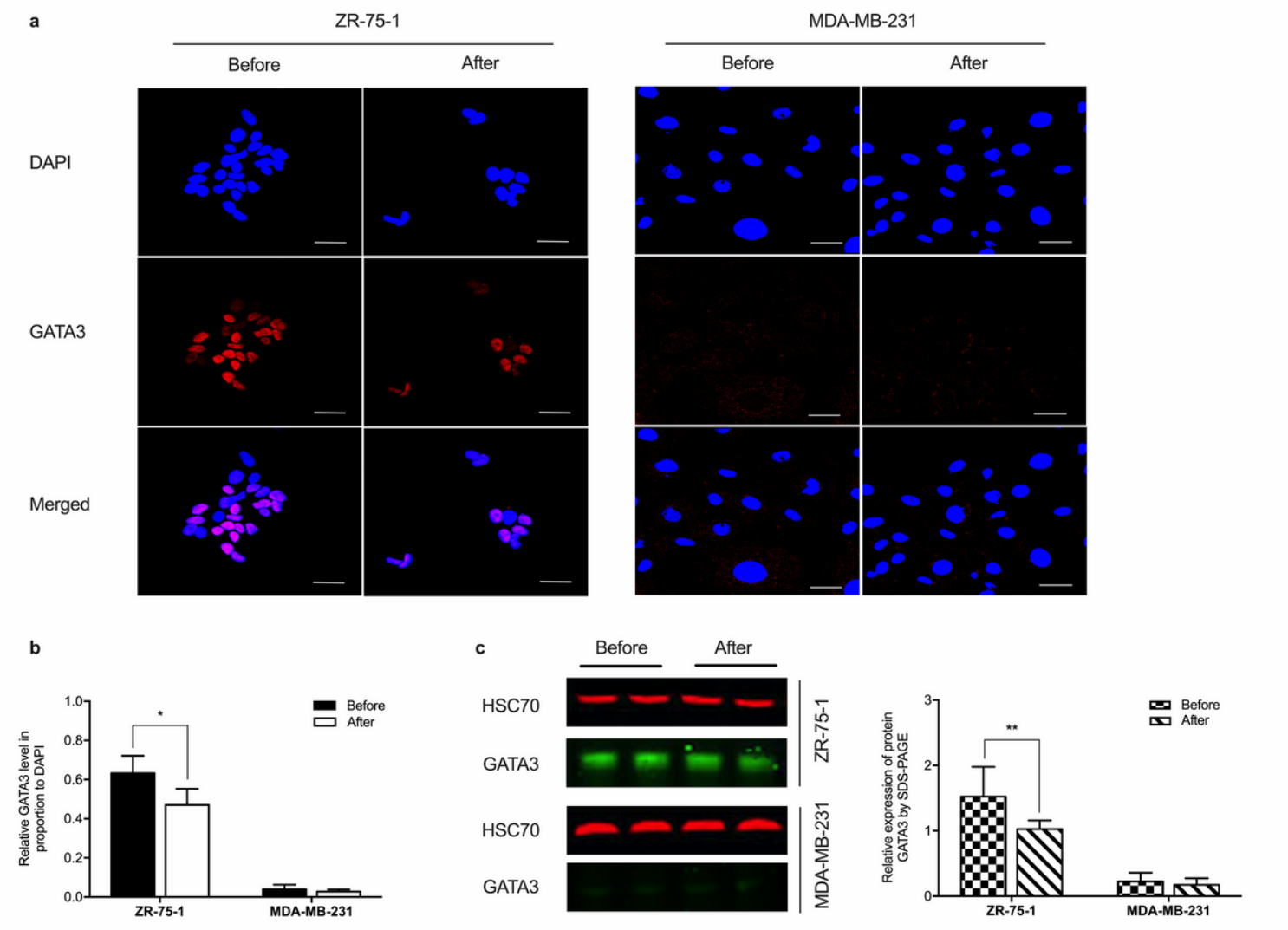

Figure 3

Downregulated expression of GATA3 in cryopreserved breast cancer cells. a Immunofluorescence images of GATA3 expression in ZR-75-1 and MDA-MB-231 cells before and after cryopreservation. Scale bar: 50 μm; b Statistical comparison of GATA3 expression in both cell lines. Significantly different at *p<0.05. c Western blotting images (left panel) and the graphical representation (right panel) of GATA3 expression in ZR-75-1 and MDA-MB-231 cells. Theses blots were cropped. Full-length gels/blots are presented in Supplementary Fig.1 (ZR-75-1 cells No.1) and Fig.4 (MDA-MB-231 cells No. 1), respectively.HSC70 was used as the control.Significantly different at **p<0.01.

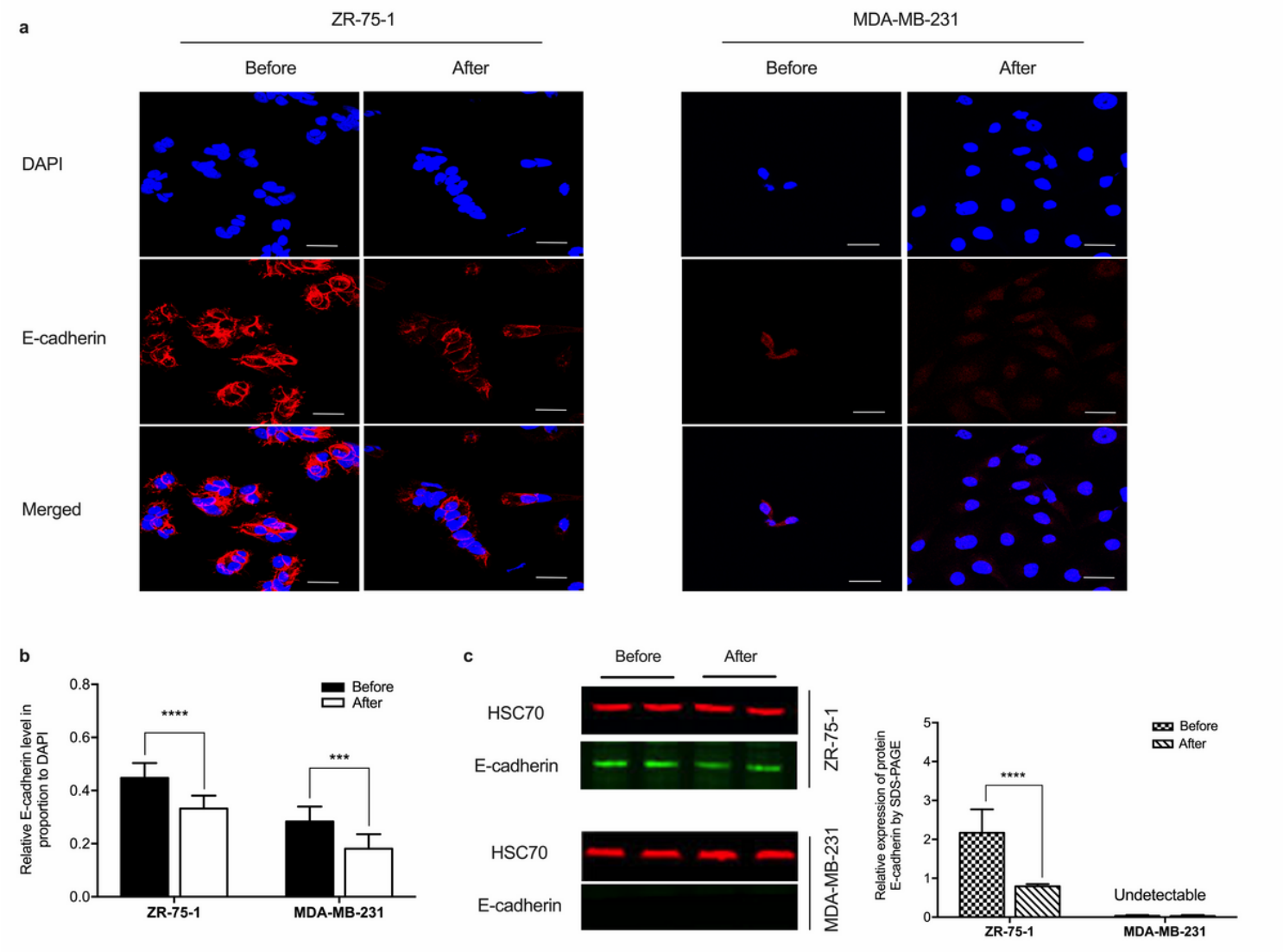

Figure 4

Downregulated expression of E-cadherin in cryopreserved breast cancer cells. a Immunofluorescence images of E-cadherin expression in ZR-75-1 and MDA-MB-231 cells before and after cryopreservation. b Statistical comparison of E-cadherin expression in both cell lines. Significantly different at ***p<0.001, ****p<0.0001. c Western blotting images (left panel) and the graphical representation (right panel) of E-cadherin expression in ZR-75-1 and MDA-MB-231 cells. Theses blots were cropped. Full-length gels/blots are presented in Supplementary Fig. 1 (ZR-75-1 cells No.1) and Fig.5 (MDA-MB-231 cells No. 2, the middle four lanes), respectively.Significantly different at ****p<0.0001.

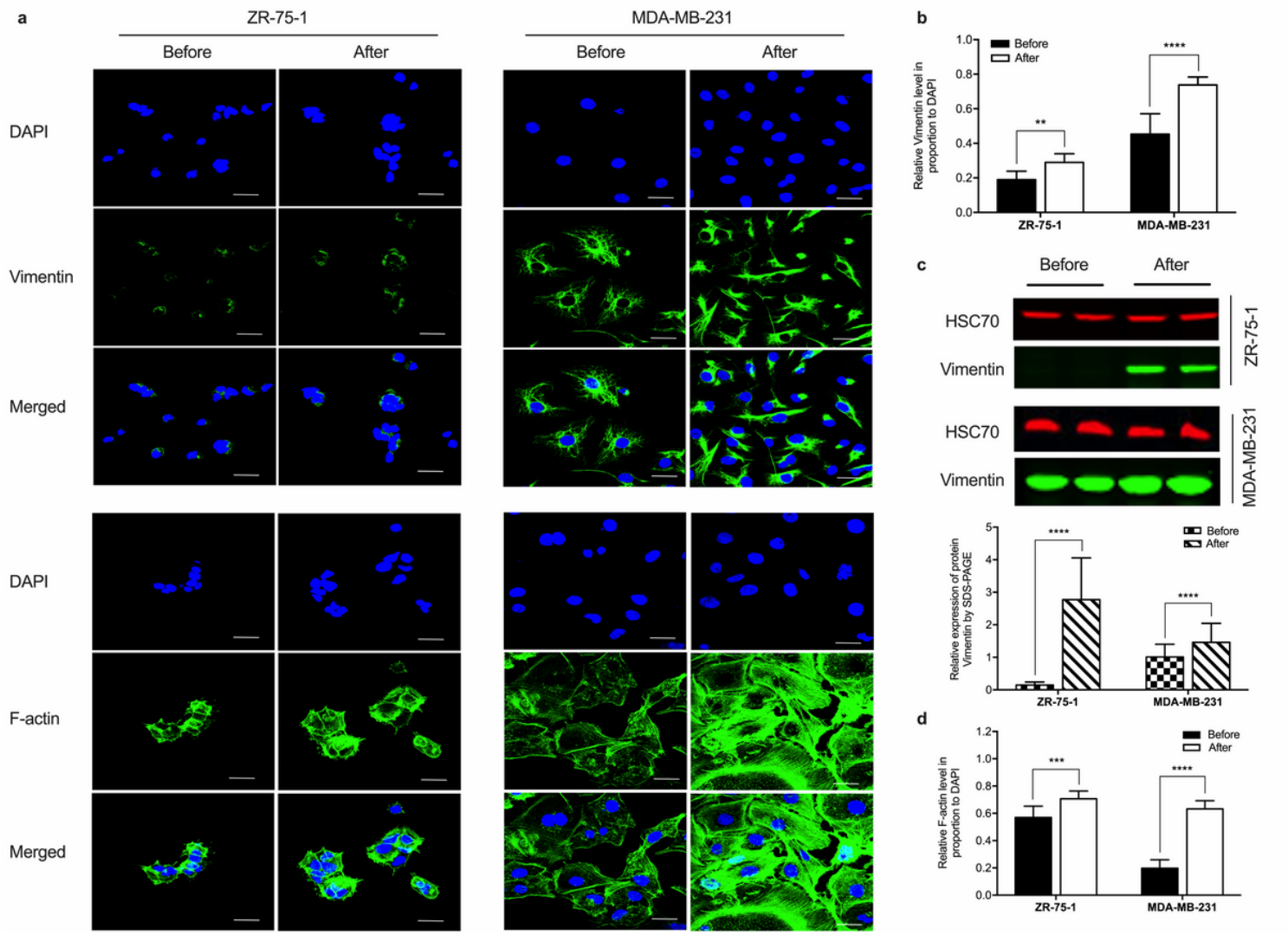

Figure 5

Upregulated expression of Vimentin and F-Actin in cryopreserved breast cancer cells. a Immunofluorescence images of Vimentin and F-Actin expression in ZR-75-1 and MDA-MB-231 cells before and after cryopreservation. b Graphical representation of Vimentin expression in both cell lines. Significantly different at **p<0.01, ****p<0.0001. c Western blotting images (upper panel) and the graphical representation (lower panel) of Vimentin expression in ZR-75-1 and MDA-MB-231 cells. Theses blots were cropped. Full-length gels/blots are presented in Supplementary Fig. 1 (ZR-75-1 cells No.1) and Fig.4 (MDA-MB-231 cells No. 1), respectively.Significantly different at ****p<0.0001. d Graphical representation of F-Actin expression in both cell lines. Significantly different at ***p<0.001, ****p<0.0001.

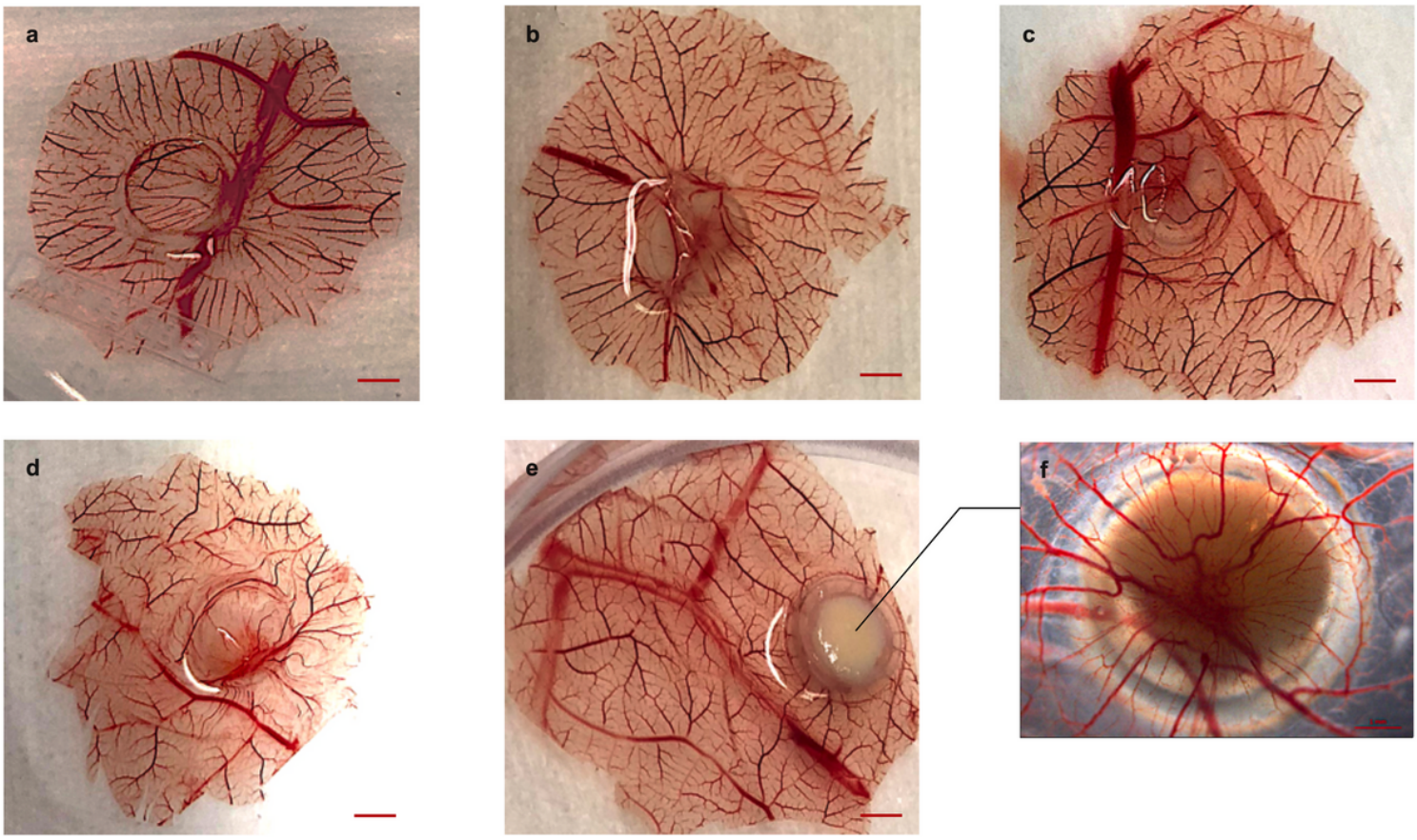

Figure 6

Increased angiogenesis after CAM-Xenotransplantation of cryopreserved cancer cells.a Negative control: 40 µl 1X Phosphate-Buffered Saline;b Representative sample of group 1: 4×106 fresh cells;c Representative sample of group 2: 8×106 fresh cells;d Representative sample of group 3: 4×106 cryopreserved cells;e Representative sample of group 4: 8×106 cryopreserved cells;Scale bar: 2.5 mm.fThe reverse side of sample in (e), scale bar: 1 mm. It was detected numerous radically distributed vasculature and vertically growth into the tissues, which was indicated by the reddishness at the middle of the transplanted sites.

Supplementary Files

This is a list of supplementary files associated with this preprint. Click to download.

- SupplementaryFig.6.MDAMB231cellsround3.tiff
- SupplementaryFig.5.MDAMB231cellsround2.tiff
- SupplementaryFig.4.MDAMB231cellsround1.tiff
- SupplementaryFig.3.ZR751cellsround3.tiff
- SupplementaryFig.2.ZR751cellsround2.tiff
- SupplementaryFig.1.ZR751cellsround1.tiff

- Supplementaryfig.7Thecroppedblots.tiff